

Important Notice to Authors

No further publication processing will occur until we receive your response to this proof. Please respond within 48 hours of receipt of this message.

Ways to Respond

- Web: If you accessed this proof online, follow the instructions on the web page to submit corrections.
- Email: Send corrections and other questions to spie-manager@luminad.com. Include the paper ID number in the subject line.

Items to Address

A list of questions and comments for you to address is on the last page of this pdf. In addition:

- Proofread the article carefully. This is your only opportunity to provide corrections.
- Check title, author list, and acknowledgments carefully for any omissions or errors.
- Check text, figures, captions, equations, tables, and references thoroughly. Figure quality in this proof is representative of the quality to be used in the online version. Ensure that figure captions and text clearly describe figures.
- If you are adding biographies, note that they should not exceed 75 words each.
- Submit the publication license (if you have not already) by logging into your account at <https://oe.msubmit.net>
- If you have already paid your open access fee, thank you. If you have not yet paid or received an invoice for your open access fee, contact SPIE at journals@spie.org. If you are not publishing with open access, no fee is due.



Analysis of an active and passive optical fronthaul with dense wavelength division multiplexing for coexisting 4G/5G cloud radio access network architectures based on software defined radio

Mario Alberto Hernández-Flores,^a Miguel Cervantes-Vázquez[Ⓜ],^b
David López-Mata[Ⓜ],^b Kevin Guillermo Miceli-Ruiz,^a
Irving Rendón-Salgado,^b Mauricio Guarneros-Lozano,^b
José Bernardo Rosas-Fernández,^c Daniel Enrique Ceballos-Herrera[Ⓜ],^{b,*}
Víctor Rangel-Licea,^a and Ramón Gutiérrez-Castrejón[Ⓜ]^b

^aUniversidad Nacional Autónoma de México (UNAM), School of Engineering,
Edificio Q-Valdes Vallejo, Mexico City, Mexico

^bUniversidad Nacional Autónoma de México (UNAM), Institute of Engineering,
Mexico City, Mexico

^cMinistry of Education, Science, Technology and Innovation,
Government of Mexico City, Mexico City, Mexico

Abstract We experimentally investigate the performance of an active and passive optical fronthaul to be employed in a cloud/centralized radio access network (C-RAN) architecture based on software-defined radio (SDR) for 4G systems, and we discuss the viability to integrate these fronthaul configurations in coexisting 4G/5G systems based on SDR by considering the reconfigurable characteristics of SDRs and the capacity and latency characteristics of the optical fronthaul. The active optical fronthaul consists of two transponders employing dense wavelength division multiplexing (DWDM), whereas the passive optical fronthaul consists of a point-to-point scheme based on DWDM only. To perform a comparative study between the active and passive optical fronthaul in the C-RAN architecture, we have measured the throughput (bit rate) generated via iPerf[®] for uplink and downlink transmissions at different DWDM channels, and we analyze the losses and latency presented in both optical fronthaul schemes. We found that for different optical fronthaul lengths up to 21.76 km, the bit rate is practically the same for the passive and active fronthaul despite the higher optical losses present in the passive fronthaul in comparison to the active fronthaul. In addition, the latency among active and passive fronthaul are almost similar with an estimated increment of 20 μ s in the active fronthaul. These results are independently of the number of remote radio heads (RRHs) and user equipment (UEs) considered in the C-RAN architecture. Our findings put forward the proposed DWDM passive fronthaul as a viable, less complex, and cost-sensitive solution for C-RAN systems with fronthaul lengths up to 21.76 km. These results and all the experiences reported on the C-RAN implementation provide valuable information to design and develop 4G and 5G C-RAN architectures based on SDR with the capability to operate in a DWDM optical fronthaul infrastructure. © 2022 Society of Photo-Optical Instrumentation Engineers (SPIE) [DOI: 10.1117/1.OE.61.XX.XXXXXX]

Keywords: optical fronthaul; dense wavelength division multiplexing; centralized radio access network; software-defined radio; 4G/5G networks.

Paper 20220517G received May 16, 2022; accepted for publication Sep. 27, 2022.

1 Introduction

Since its inception, mobile communications networks have been experiencing continuous growth in traffic demand. According to Ref. 1, between 2019 and 2025, mobile traffic is expected to grow at an annual rate of 31%. To fulfill the future market demands, it is necessary

*Address all correspondence to D. E. Ceballos-Herrera, DCeballosH@iingen.unam.mx

to evolve from the actual 4G networks toward a new generation of mobile communications, the 5G network. During this transition, both 4G and 5G technologies must coexist adequately and satisfy together the growing connectivity demand.^{2,3} By 2025, it is expected that 5G networks will carry 45% of the total mobile data traffic. This new technology will foster new services, such as autonomous driving, augmented reality, virtual reality, and Internet of Things (IoT).^{1,4}

The future 4G/5G network deployment imposes a great variety of technological challenges, most of them related to the Radio Access Network (RAN). As a result, several solutions have been proposed. The most recent versions of 4G long-term evolution (LTE) and 5G-NR networks rely on a centralized-radio access network (C-RAN).^{5,6} In C-RANs, the mobile base station functions are distributed between the remote radio heads (RRHs) and the base band processing units (BBUs). A communication link is then defined between RRHs and BBUs, which is referred to as the fronthaul. The multiple RRHs, which are deployed closer to the end users in different geographical locations, perform the radio signal processing and generate their corresponding digital data, which are transmitted to the BBU using the fronthaul link. This digital transmission can be done using standard protocols like the common public radio interface (CPRI), the open base station architecture initiative (OBSAI), or Ethernet.^{6,7} The BBUs, located in the same central office, also called the BBU pool, receive the digital data and process the information in base-band for the next communication layers. Afterward, the BBUs are connected to the core/backbone via the evolved packet core (EPC) using a backhaul network. In general, the adoption of a C-RAN architecture offers a reduction in energy consumption due to the sharing of the base-band processing resources and the cooling infrastructure installed in the same BBU pool. It reduces the implementation costs and makes it possible for a greener infrastructure. Additionally, the opportunity to control hundreds of RRHs from the same BBU pool, improves the system mobility and facilitates the network scalability, simplifying in this way the management and operation of the fronthaul network.^{5,7,8}

The fronthaul network is one of the most important elements of the C-RAN architecture.⁹ Fiber optics and wireless technology can be used as fronthaul networks in C-RAN architectures. In particular, wireless technologies like microwaves are an alternative for short distance fronthaul networks where fiber optics is physically or economically not an option. The wireless fronthaul can be used in scenarios where an ultradense deployment of RRHs is implemented, however in this case, the fronthaul is sensitive to weather fading and its length is limited to 1 km.^{7,8} On the other hand, a fiber optic fronthaul can be implemented for long distances around 20 km, and it can offer higher bandwidths with high reliability compared to a wireless fronthaul, which is desirable in multiple dedicated services like telemedicine. Both, fiber optics and wireless can also be combined to optimize the C-RAN architecture of a cellular network.¹⁰ Among all available technologies for fronthaul deployment, optical networks are preferred due to their low latency (light propagates at around 5 $\mu\text{s}/\text{km}$) and high transmission capacity.^{11–13} Several studies have emerged to propose different optical configurations for the fronthaul, some of them focused on the use of DWDM technologies in active and passive architectures.^{14–16} In the case of active fronthaul, the information between RRHs and BBUs is transmitted using DWDM channels at wavelengths laying in the C-band. This solution, unfortunately, requires optic-electric-optic (OEO) transponders for conversion of the 1310 nm optical signals coming from the RRHs and the BBUs to DWDM signals operating at around 1550 nm and vice versa. In the case of a passive optical fronthaul, several proposals consider the current infrastructure of commercial DWDM passive optical networks (PON) composed of an Optical Line Terminal (OLT) and multiple optical network units (ONUs) distributed in coordinate multipoints (CoMP) or point-to-point (PtP) configurations. The OLT and ONUs contain optical transceivers that generate the DWDM channels to be transmitted between the BBUs and RRHs. Hence, the C-RAN is built over the PON infrastructure, which is not necessarily an optimum approach. It is then clear that there is not enough research on passive optical fronthaul configurations. In particular, those where the RRHs and BBUs directly transmit and receive the digital data traffic at DWDM wavelengths without the use of OLT and ONU components. This issue, hence, has to be explored from a deployment perspective to design passive optical fronthaul alternatives that are less complex and more cost-effective. This is one of the topics investigated in this work.

Additional research has been carried out to analyze the capabilities of time division multiplexing (TDM) in PON systems as optical passive fronthaul in C-RAN architectures. These

studies have demonstrated fronthaul bandwidths higher than 10 Gb/s and a reduction of the latency caused by the bandwidth allocation performed by the OLT to different ONUs.^{17,18} More significant improvements in bandwidth and latency have been obtained in passive optical fronthaul schemes using a combination of TDM and WDM, also named TWDM.^{19,20} Other, more advanced fronthaul proposals, rely on the use of spatial division multiplexing (SDM) over multi-core fibers (MCF),²¹ hybrid combinations of SDM and DWDM,^{22–24} and even a hybrid fiber-FSO (free-space optics) fronthaul.^{3,25} All these studies have been performed with the goal of enhancing the fronthaul flexibility to simultaneously transmit data traffic generated by different radio access technologies present in 5G and 4G networks; however, these solutions increase the deployment costs of the C-RAN architecture. In general, all these optical fronthaul schemes must meet strict bandwidth and latency constraints for 5G mobile systems that are not necessarily required in 4G. For example, the 5G optical fronthaul must support data transmission of around 100 Gb/s and must comply with a maximum total round-trip latency of up to 250 μ s between the RRH and BBU.^{25–30} If these constraints are met, the optical fronthaul can satisfy transmission scenarios where 4G and 5G networks operate simultaneously using the same optical fronthaul, a situation that will occur frequently during the gradual process of the 5G network deployment in places where 4G has a significant presence. This 4G/5G coexistence is also consequence of the release 15 specifications of the third generation partnership project (3GPP), which states that the initial 5G deployments will be based on a nonstandalone (NSA) architecture, with a partial reuse of the legacy 4G-LTE infrastructure in combination with multiple radio access technologies.³¹

From the statements mentioned above, it results natural to analyze how the optical transport in C-RAN architectures can be reconfigured at the lowest possible cost, to simultaneously operate in 4G and 5G, or only in 5G, according to the mobile traffic demand present in the coverage area. An appealing approach to design and implement flexible and reconfigurable C-RAN architectures is the use of virtual machines for the RAN and core elements, which simplify and reduce the deployment and operation cost of mobile networks. This virtualization of network elements allows for a scalable network that improves the resource utilization.^{5,32,33} Software-defined networks (SDNs) are one alternative to implement this virtualization. According to the SDN concept, resources in each network segment, i.e., radio and transport, are managed in a control plane without the involvement of the management interfaces.^{34,35} In this way, the SDN platform can reconfigure paths to divert the traffic between the RRUs and BBUs, without having to send engineers to sites. In the SDN, the key elements of 4G and 5G networks, like RRH's, BBU's, and the EPC, are programmed in software-defined hardware, preferably using open source software provided by initiatives like open air interface (OAI³⁶) or software radio system (SRS³⁷), which are in compliance with the 3GPP standards.^{32,38} Both are feasible and stable platforms for implementing software-defined 4G/5G RAN.^{32,39} In particular, the SRS software is more modular and easier to customize than OAI, but OAI is more computationally efficient than SRS.³⁹ Additionally, both software can run on general computing platforms (x86) together with off-the-shelf (OTS) software-defined radios (SDRs). A relevant example of SDR equipment family that is suitable to develop 3GPP cellular networks is the ETTUS[®] Research Universal Software Radio Peripheral (USRPs),⁴⁰ which can interoperate with commercial equipment and transmit digital data with CPRI and Ethernet protocols.^{41,42} The use of this flexible alternative makes the implementation of compliant 4G and 5G mobile networks more accessible at industrial and academic levels; however, the SDN technology is at the beginning of a long evolution road and further investigation must be performed to explore the capabilities of SDN to operate 4G and 5G mobile networks. To contribute to this continuous progress in SDN research, it results important to investigate the performance of 4G/5G C-RAN architectures based on SDR by considering different optical fronthaul configurations and exploring the capabilities of SDN, thus achieving a flexible and reconfigurable low-cost operation of coexisting 4G/5G C-RAN architectures to manage a variety of mobile traffic demands.

Under this context, in this paper, we experimentally investigate the operation of an active and passive optical fronthaul based on DWDM in a 4G C-RAN architecture based on SDR. Moreover, we discuss how these architectures can also be employed in future coexisting 4G/5G systems by considering the reconfigurability of SDRs and the capacity and latency characteristics of the active and passive DWDM optical fronthaul. The principal contributions originated from this study can be summarized as follows:

1. A comparative analysis of a passive and active DWDM optical fronthaul using different fiber lengths of up to 21.76 km for coexisting 4G/5G C-RAN architectures based on SDR. This comparative analysis using different optical fronthaul lengths in C-RAN architectures based on SDR has not been reported before.
2. A proposal of DWDM passive optical fronthaul, where the RRHs and BBUs directly transmit and receive the digital data traffic at DWDM wavelengths without the use of OLT and ONU components, can serve as a viable, less complex, and cost-sensitive solution for C-RAN systems based on SDR with fronthaul lengths up to 21.76 km.
3. Assessment of the capabilities of SDR to implement a flexible and reconfigurable low-cost operation of coexisting 4G/5G C-RAN architectures considering a variety of mobile traffic demands produced by the interconnection of multiple UEs to different USRP radios. To the best of our knowledge, this is the first formal study to address this investigation.

The paper is organized as follows. In Sec. 2, we present the proposed active and passive C-RAN architectures and their corresponding experimental setup, where the optical and radio systems are detailed. In Sec. 3, we present the optical characterization of the active and passive DWDM fronthaul. In Sec. 4, we demonstrate the technical feasibility of both active and passive fronthaul to be used in C-RAN architectures by evaluating their performances through bit rate measurements between the RRHs and the BBUs for downstreams and upstreams transmissions. In Sec. 5, we discuss the comparison between the active and passive DWDM optical fronthaul and the viability to integrate these fronthaul configurations in coexisting 4G/5G C-RAN architectures based on SDR. Finally, we present our conclusions in Sec. 6.

2 Proposed C-RAN Architectures

In this contribution, we consider two options of C-RAN architectures. The first one contains an active optical fronthaul based on DWDM technology as it is presented in Fig. 1. In this option, the optical fronthaul is based on the use of 10G transponders that convert the optical signals generated by the SFP+10GBASE-LR transceivers, operating at 1310 nm, to DWDM wavelengths spectrally located in C-band and vice versa. The DWDM lanes are separated 200 GHz. The setup also relies on the use of MUX/DEMUX passive optical components that allow the

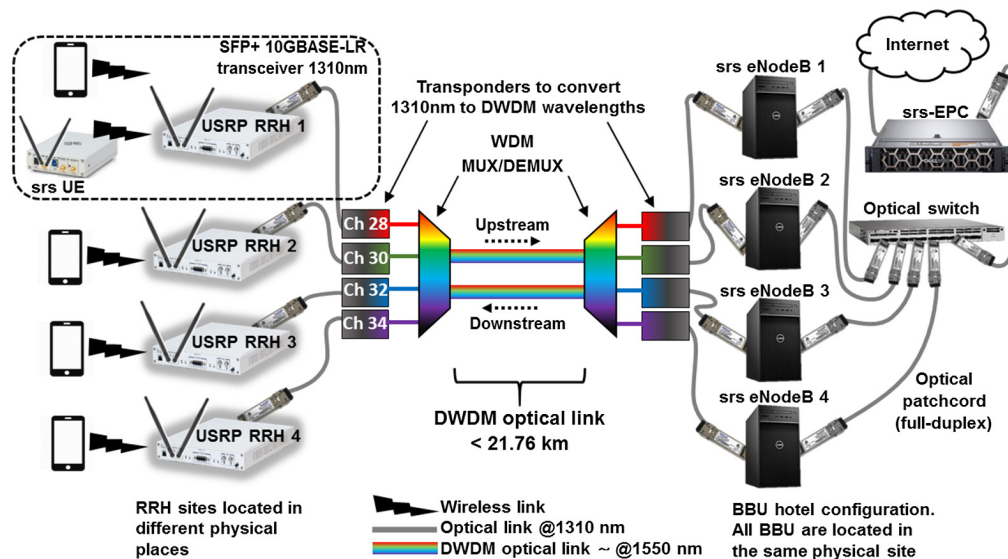


Fig. 1 Setup for the C-RAN architecture with an active optical fronthaul. Two optical transponders in the upstream and downstream directions are employed to convert the optical signals at 1310 nm (gray lines) to different DWDM channels (colored lines) and vice versa. Four DWDM channels are transmitted in the active optical fronthaul: Ch. 28, $\lambda = 1554.94$ nm, Ch. 30, $\lambda = 1553.32$ nm, Ch. 32, $\lambda = 1551.72$ nm, and Ch. 34, $\lambda = 1550.10$ nm.

transmission of DWDM channels along the G.652-compliant full-duplex optical link that interconnects the RRHs and their corresponding BBUs, also called eNodeBs and gNodeBs in 4G and 5G configurations, respectively. In our setup, the DWDM optical link length can be gradually incremented to reach up to 21.76 km to evaluate the effects of the optical fronthaul length in the 4G and 5G network performance.

As it is shown in Fig. 1, the RRHs consist of software-defined radios (Ettus Research X310) that employ the USRP hardware. 10G Ethernet interfaces perform digital optical communication to the eNodeB.³⁹ Due to availability, we only considered four RRHs, but this quantity can be scaled in accordance with the maximum quantity of DWDM channels supported by the optical fronthaul. In the same way, the corresponding four eNodeBs are implemented in four Dell Precision 3630 desktop computers (Intel Core i7) running Ubuntu 16.04.6 LTS together with an ixgbe 5.1.0-k controller. The EPC is implemented in a Dell Precision R7920 server (Intel Xeon Bronze 3204) and interconnected to the eNodeBs using a 10GbE optical switch and multiple full-duplex optical patch cords operating with gray ($\lambda = 1310$ nm) optics. The RRH, eNodeB, and EPC are then based on the software-defined network (SDN) paradigm, and their functions are programmed using the open source SDR 4G/5G software suite provided by SRS,⁴³ Release srsLTE 20.04.⁴⁴ Finally, in the proposed setup, we have employed commercial cell-phones (Xiaomi[®] Redmi 9A) as user equipments (UEs), and a software-defined radio (Ettus Research B210) as an additional UE, whose functions were also programmed in Ubuntu OS using the srsLTE software and a Dell G7 laptop. In this way, we can analyze the network performance of the C-RAN architecture based on SDR using two different types of UEs, as it is shown in Fig. 1 for RRH 1.

For the second option of SDR-based C-RAN architecture, we have considered a passive optical fronthaul based on DWDM technology. It is presented in Fig. 2. In this option, the optical signals at DWDM wavelengths (C-band) are directly generated by the SFP+ 10GBASE-ER transceivers plugged into the network interface cards installed on the RRHs and eNodeBs. This C-RAN architecture does not require active components along the optical fiber link to transmit the DWDM channels. Hence, with respect to the active solution, the passive option represents a less complex and less expensive solution. It still requires, however, the use of a passive MUX/DEMUX pair as shown in Fig. 2. The DWDM optical link length of the passive option can also be gradually incremented to reach 21.76 km. We have also considered four RRH's with their corresponding four eNodeBs, which in turn are connected to the EPC as in the active solution. The RRHs, eNodeBs, and EPC are also programmed in Ubuntu OS using the open source

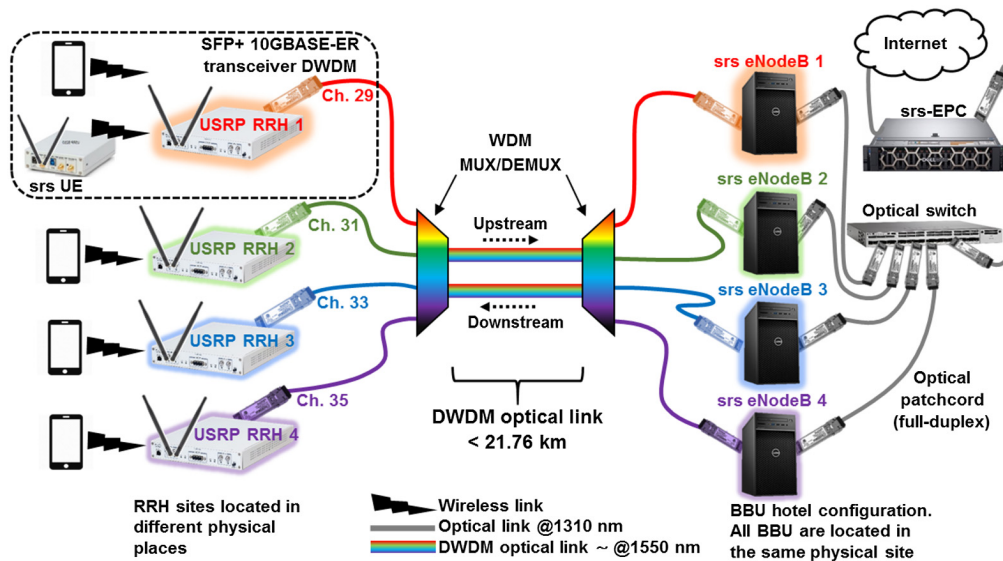


Fig. 2 Setup for the C-RAN architecture with a passive optical fronthaul. No optical active equipment is required to convert and transmit DWDM channels (colored lines) through the optical link. Four DWDM channels are considered: Ch. 29, $\lambda = 1554.13$ nm, Ch. 31, $\lambda = 1552.52$ nm, Ch. 33, $\lambda = 1550.91$ nm, and Ch. 35, $\lambda = 1549.31$ nm.

Table 1 RF and optical equipment.

| Equipment | Quantity | Description |
|--|----------|--|
| USRP RRH | 4 | USRP Ettus Research X310, Ref. 41 |
| USRP UE | 1 | USRP Ettus Research B210, Ref. 42 |
| Cellphone UE | 8 | Xiaomi Redmi 9A |
| Antennas | 10 | VERT2450 for TX and RX with 3 dBi gain from Ettus Research |
| eNodeB | 4 | Intel Core i7-9700 (eight cores, eight threads) @ 3 GHz, 16 GB of DDR4 RAM |
| Optical switch | 1 | Catalyst WS-C3850-24XS-S from Cisco® |
| EPC | 1 | Workstation Dell Precision R7920 |
| Optical fiber | 21.7 km | Standard single monomode fiber (ITU-T G.652.D), Ref. 46 |
| DWDM MUX/DEMUX | 2 | With capacity to multiplex up to eight DWDM channels: 28, 29, 30, 31, 32, 33, 34, 35 from PacketLight® |
| Optical transponders (optical-electrical-optical converters) | 2 | PL1000TE from PacketLight® |
| Network interface card | 8 | Dual SFP+ Ports @10 Gbps with 10GBASE-ER and 10GBASE-LR support from Intel® |
| Transceiver (colored optics) | 8 | SFP+ 10GBASE-ER DWDM channels 28,30,32,34 from PacketLight®, channels 29 and 33 from SolidOptics® and channels 31 and 35 from SmartOptics® |
| Transceiver (gray optics) | 18 | SFP+ 10GBASE-LR @1310 nm from Intel® or Finisar® |
| Optical Patchcords | 13 | 10 m length with LC UPC connectors |

srsLTE software. It is important to mention that the DWDM channels transmitted in the passive fronthaul correspond to channels 29, 31, 33, and 35, spaced 200 GHz apart. In contrast, the DWDM channels transmitted in the active fronthaul correspond to channels 28, 30, 32, and 34. All these channels follow the nomenclature based on the ITU-T G.694.1 recommendation for the DWDM frequency grid.⁴⁵ This different selection of DWDM channels transmitted in the active and passive fronthaul arises from the fact that, with this choice, it is possible to set up in the future a hybrid configuration using an active and passive optical fronthaul simultaneously and transmit up to eight DWDM channels through the optical link. In this sense, it is worth mentioning that the employed optical transponders and the MUX/DEMUX components can support up to eight DWDM channels, from channel 28 to 35. In this work, we separately present the analysis of both individual architectures (active and passive).

Table 1 shows more details about the radio frequency (RF) and optical equipments employed in both proposed C-RAN architectures. Special mention must be made to the transceivers and network interface cards because these must be properly selected to be compatible. According to our experience, the network interface card Ethernet X520-LR2 provided by Intel® can operate correctly with the following gray transceivers SFP+ 10GBASE-LR @1310 nm: FTLX1471D3BCV-IT from Intel®, and FTLX1472M3BCL from Finisar®, as well as, it can also operate with colored transceivers SFP+ 10GBASE-ER DWDM provided by SmartOptics® and SolidOptics®. Additionally, the network interface cards are installed on the USRP radios and PC's using their respective PCI Express x16 v2.0 slots.

3 Characterization of Optical Components

To continue with the description of the proposed architectures, it is important to remark that the principal interest of this work is to analyze and compare the operation of an active and a passive optical fronthaul based on DWDM in the C-RAN architecture based on SDR. In this sense,

it is important to characterize the optical components employed in both active and passive fronthaul networks.

3.1 Optical Transceivers

With respect to the gray transceivers, these are only employed to transmit 1310 nm optical signals along short optical patch cords of 10 m length, which are identified as gray lines in Figs. 1 and 2. As a consequence, no problems are found in the C-RAN performance caused by these transceivers. In particular, the gray transceivers SFP+10GBASE-LR contain a distributed feedback (DFB) diode laser as transmitter and a PIN photodiode as an optical receiver. To verify the correct operation of the DFB laser of these gray transceivers, we also performed measurements of the transmitter output power using an optical power meter and we obtained output power values between -3.94 and -2.11 dBm, which fall within the allowed ranges specified in their respective datasheets.

With respect to the colored optical transceivers SFP+ 10GBASE-ER DWDM, which transmit at the DWDM channels 28 to 35, these contain an electro-absorption modulated laser (EML) as transmitter and a PIN photodiode as an optical receiver. It is important to consider that these optical signals pass through the filters that correspond to the MUX/DEMUX components, and are transmitted up to 21.76 km along the DWDM optical link. Therefore, it is crucial to verify in this case the correct operation of each of these DWDM transceivers in relation to their output power, emission wavelength, and linewidth. Then, we perform laser optical power measurements at the output of the EML lasers of each DWDM colored transceiver obtaining optical power values ranging from 0.3 to 2.11 dBm. Again, all these power values lie within the allowed ranges specified in their datasheets. In addition, we perform spectral measurements of the DWDM signals emitted by these transceivers to analyze their emission wavelength and 3 dB linewidth. In this case, the spectral measurements were carried out after the MUX/DEMUX components in both upstream and downstream directions using an Anritsu[®] MS9740A optical spectrum analyzer (OSA). We obtained the results shown in Figs. 3(a) and 3(b), which correspond to the four DWDM channels transmitted in the active and passive fronthaul in upstream direction, respectively. Similar spectral results are obtained in downstream direction. In Fig. 3, we can visualize the DWDM channels at the beginning of the optical link, just after the MUX component (blue curves), and at the end of the optical link with 21.7 km of fiber length, just before the DEMUX component (red curves). According to the spectral measurements shown in Fig. 3, the emission wavelengths of the colored transceivers coincide with the DWDM channels 28, 30, 32, and 34 for the active optical fronthaul, and with the DWDM channels 29, 31, 33, and 35 for the passive optical fronthaul; however, slight differences in emission wavelength lower than 0.08 nm are presented in both cases. In addition, the 3 dB linewidth measurements obtained from Fig. 3 for all DWDM channels transmitted in the active and passive fronthaul present values between 0.05 and 0.09 nm, which also lie within the allowed ranges described in their respective datasheets. In these measurements, the OSA wavelength resolution was set to 0.03 nm. Additionally, from the spectral measurements, we have calculated the optical signal-to-noise ratio (OSNR) of each DWDM channel after the MUX component, i.e., just at the beginning of the DWDM optical link (see blue curves in Fig. 3). Excellent OSNR values within the range of 55 to 56 dB for the active fronthaul, and OSNR values within the range of 55 dB to 57 dB for the passive fronthaul, were measured. In general, the DWDM channels do not present distortion at the end of the optical fiber caused by nonlinear fiber effects and their OSNR values are not modified along the optical link (see red curves in Fig. 3). This behavior is expected considering the low input powers and the high channel spacing (200 GHz) employed in the DWDM optical transmission experiments, even when 21.76 km of fiber were employed. The negligible nonlinear effects observed in our WDM measurements are in accordance with Ref. 47, where four DWDM channels spaced 200GHz apart were transmitted along a fronthaul length of 20km using a standard single-mode fiber (SSMF), similar to the one employed in our fronthaul link. In this scenario, an optical power per DWDM channel of 10.5 dBm is required to appreciate four-wave-mixing (FWM) and cross-phase modulation (XPM) effects among all DWDM channels in C-Band. This is not our case because the maximum optical power measured for the colored DWDM transceivers used in our experiment was +2.11 dBm, launched into an optical link exhibiting

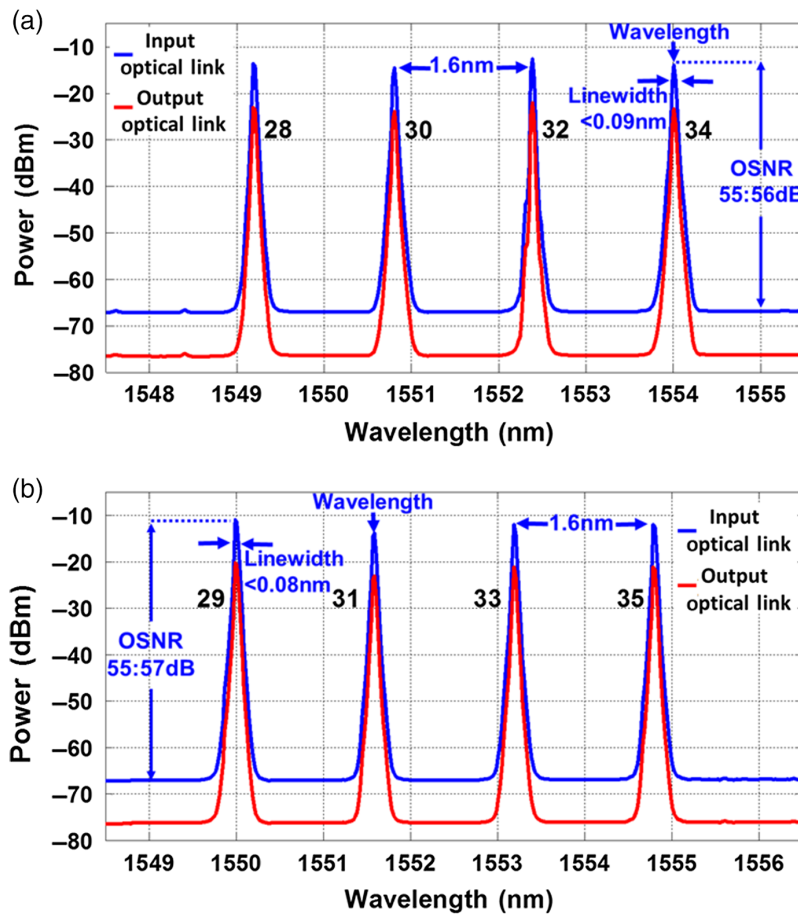


Fig. 3 Spectral measurements of four DWDM channels transmitted in the (a) active (even channels) and (b) passive (odd channels) optical fronthaul. The measurements were acquired after the multiplexer (MUX) in the upstream direction. Similar spectral measurements are obtained for the downstream direction. Blue and red curves correspond to DWDM channels at the beginning and at the end of the optical link with 21.76 km of fiber length. The DWDM channels are spaced 200 GHz (1.6 nm) apart.

high losses. Similarly, we can also expect low power penalties due to chromatic dispersion effects for each DWDM channel. This is due to the fact that for NRZ transmission at 10 Gb/s in an SSMF fiber at around 1550 nm, a fiber length of ~ 70 km is required to obtain a dispersion power penalty of 1 dB,⁴⁸ which is far too long as compared with the fiber length used in our testbed.

According to Fig. 3, by comparing the spectral powers of the blue and red curves, we can estimate the loss that presents each DWDM channel transmitted along 21.7 km of fiber length, which is 9.2 dB for upstream direction. In the case of downstream direction, this loss is 9.4 dB. These loss measurements correspond only to the optical fiber link and do not include the insertion loss (IL) of the MUX/DEMUX components. To consider these IL, we carried out optical power measurements of each DWDM channel before and after the MUX/DEMUX component and by comparing these power measurements, we obtained IL values of 2.5 dB for each component. It indicates that the losses of each DWDM channel in the complete fronthaul scheme, including those pertaining to the optical fiber link and both MUX/DEMUX components, can reach 14.2 and 14.4 dB in the upstream and downstream directions, respectively.

3.2 Optical Fiber Link

In order to verify and describe in detail the losses and attenuation present in the full-duplex DWDM optical fiber link, we perform measurements using an optical time domain reflectometer

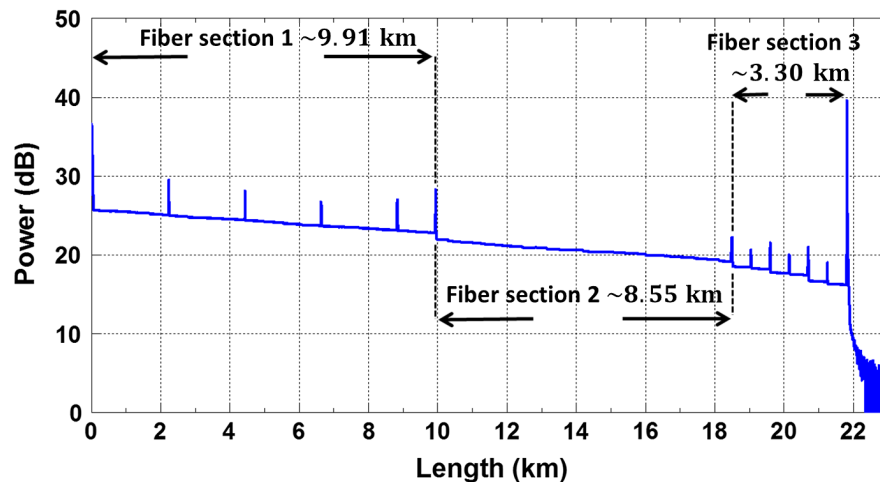


Fig. 4 OTDR trace of the fiber link in the upstream direction. The optical fronthaul is composed of three different fiber sections joined together with mechanical connectors. The maximum fiber length is 21.76 km with an accumulative loss of 9.2 dB. These measurements do not consider the insertion loss of the MUX/DEMUX components.

(OTDR) in upstream and downstream directions. In the OTDR settings we select 1550 nm as the operation wavelength, and 100 ns as pulse width. The OTDR trace for the optical fiber link used for upstream transmission is shown in Fig. 4. According to this trace, we can identify three principal optical fiber sections, the first one, 9.91 km long, the second one, 8.55 km long, and the last one, 3.3 km long. These three fiber sections are joined together using fiber optics mechanical connectors. This particular configuration allows us to modify the optical fiber link according to the following lengths: 9.91, 18.46, and 21.76 km. In this way, we can evaluate the effects of the optical fronthaul length on the network performance of the proposed C-RAN architecture. For this specific OTDR trace, we can measure an accumulative loss of 9.2 dB along the 21.76 km of optical fiber. It verifies the previous fiber link loss measurement obtained with the OSA in the upstream direction. This excessive loss is mainly caused by the multiple mechanical splices placed inside the first and third fiber sections. Note that the second fiber section contains multiple fusion splices that do not generate optical reflections. Although this poorly spliced fiber infrastructure is, perhaps, not commonly found in ad-hoc fronthaul deployments, we decided to work with it because it represents an interesting worst-case scenario that operators might find in practice. At this point, it is important to remark on the importance of maintaining the optical fiber connectors clean in all the mechanical splices found in the optical link, because according to our experience, a dirty or contaminated connector can produce a network failure, mainly when dealing with fiber lengths longer than 20 km, like the one employed in the present work. It is important to note again that all these OTDR measurements only consider the optical link up to 21.7 km of fiber length and do not include the MUX/DEMUX IL.

The downstream transmission OTDR trace is shown in Fig. 5. There we can identify again three optical fiber sections with the same lengths reported in Fig. 4, but with different losses caused by the mechanical and fusion splices. For this specific OTDR trace, we can measure an accumulative loss of 9.4 dB along the 21.76 km of fiber, which is close to the accumulative loss reported in Fig. 4. Again, the accumulative loss of this OTDR trace verifies the previous fiber link loss measurement obtained with the OSA for the downstream direction. We also found that this imbalance in the accumulative losses of 9.2 and 9.4 dB in the optical link for upstream and downstream transmissions, respectively, does not affect the network performance of the C-RAN architecture, as will be shown in the next section.

4 Performance Evaluation Results

In this section, we evaluate the network performance of the C-RAN architecture using the active and passive DWDM optical fronthaul. It consists of measuring the throughput (bit rate)

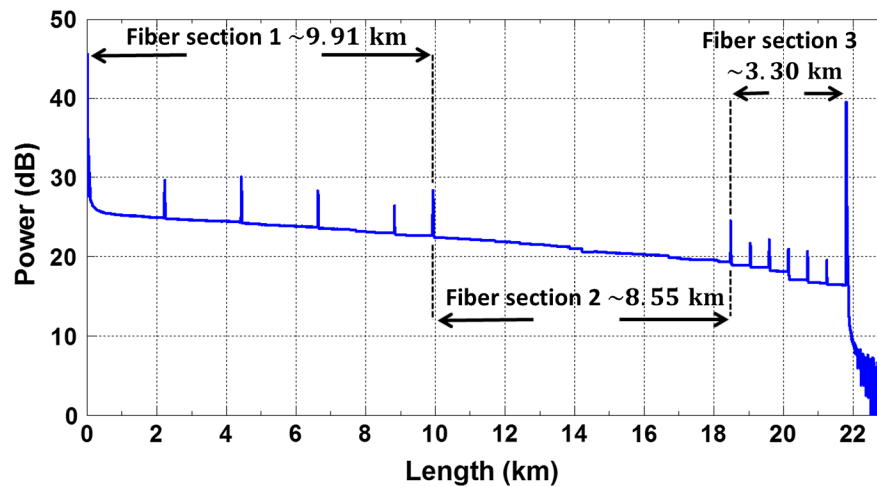


Fig. 5 OTDR trace of the fiber link in the downstream direction. The optical fronthaul is composed of three different fiber sections that can be joined using mechanical connectors. The maximum fiber length is 21.76 km with an accumulative loss of 9.4 dB. These measurements do not consider the insertion loss of the MUX/DEMUX components.

transmitted in the cellular network for upstream and downstream transmissions. The data traffic is generated using the tool iPerf[®], which is an open-source traffic generation module that runs in Ubuntu and other operating systems. It allows us to obtain data transfer characteristics like the bandwidth and throughput of a cellular network,⁴⁹ and it has been used in other studies for evaluating the throughput in SDR 4G/5G networks.⁵⁰⁻⁵² Particularly, the bidirectional data transfers (from EPC to UEs, i.e., the downstream transmission, and UEs to EPC, i.e., the upstream transmission) using the transfer control protocol (TCP) were performed for 2 min, and they were repeated four times in order to obtain an average value. In addition, it is possible to obtain a theoretical throughput based on the LTE (long-term-evolution) standard by following the procedure described in Ref. 53, which involves different parameters of the LTE physical layer (PHY), like the modulation coding scheme (MCS), bandwidth (BW), and resources blocks (RBs), among others. In this way, we can perform a comparison between theoretical and measured throughput for upstream and downstream transmissions in the C-RAN architecture. In these calculations, we consider typical BW values of 10 and 15 MHz supported by the URSP devices and employed in 4G-LTE systems, however, the 20 MHz BW channel of 4G-LTE was no possible to test due to signal processing limitations of the USRP devices. For consistency, and to avoid the introduction of external factors to the fronthaul evaluation, in all measurements, the separation between the UE and the RRH considered in this work was set to 1 m. Additionally, the optical fronthaul length can be varied from 0 to 21.76 km. Once we have considered these conditions, we can proceed to measure the throughput using the active and passive optical fronthaul.

As a first step, we perform the throughput measurements using the USRP (Ettus Research B210) as UE connected to the RRH 1. The results of the theoretical and measured throughput for different active and passive fronthaul lengths are shown in Tables 2 and 3 for downstream and upstream transmissions, respectively. The bandwidth was set to $BW = 10$ MHz. In this scenario, the DWDM channel 28 (29) is used in the active (passive) fronthaul to communicate the RRH 1 with the eNodeB 1 (Figs. 1 and 2).

Similarly, the results of the theoretical and measured throughput for downstream and upstream transmissions, now using a $BW = 15$ MHz, are shown in Tables 4 and 5.

According to the results shown in Tables 2 and 3 for a $BW = 10$ MHz, and Tables 4 and 5 for a $BW = 15$ MHz, we can state that the measured throughput in downstream and upstream transmissions does not depend on the fronthaul length, irrespective of the configuration, that is, passive or active. Consequently, for a given table, the deviation between theoretical and measured throughput remains practically the same at different fronthaul lengths. Clearly, as expected by design, the throughput in the upstream direction for both BW values is lower than the throughput

Table 2 Throughput for **downstream** transmission using a radio as UE in the C-RAN architecture with an active and passive optical fronthaul with different fiber lengths. The UE consists of a radio (USRP B210) that transmits to the RRH 1 with a **BW = 10 MHz** channel. A comparison between theoretical and measured throughput is also shown.

| Optical fronthaul length (km) | Measured throughput in the cellular network (Mb/s) | Theoretical throughput based on the LTE standard (Mb/s) | Percent deviation between theoretical and measured throughput (%) |
|-------------------------------|--|---|---|
| Passive optical fronthaul | | | |
| 0 | 34.93 | 38.01 | 8.10 |
| 9.91 | 34.93 | 38.01 | 8.10 |
| 18.46 | 35.03 | 38.01 | 7.84 |
| 21.76 | 34.93 | 38.01 | 8.10 |
| Active optical fronthaul | | | |
| 0 | 34.93 | 38.01 | 8.10 |
| 9.91 | 35.03 | 38.01 | 7.84 |
| 18.46 | 35.03 | 38.01 | 7.80 |
| 21.76 | 34.93 | 38.01 | 8.104 |

Table 3 Throughput for **upstream** transmission using a radio as UE in the C-RAN architecture with an active and passive optical fronthaul with different fiber lengths. The UE consists of a radio (USRP B210) that transmits to the RRH 1 with a **BW = 10 MHz** channel. A comparison between theoretical and measured throughput is also shown.

| Optical fronthaul length (km) | Measured throughput in the cellular network (Mb/s) | Theoretical throughput based on the LTE standard (Mb/s) | Percent deviation between theoretical and measured throughput (%) |
|-------------------------------|--|---|---|
| Passive optical fronthaul | | | |
| 0 | 12.80 | 15.10 | 15.23 |
| 9.91 | 12.80 | 15.10 | 15.23 |
| 18.46 | 12.80 | 15.10 | 15.23 |
| 21.76 | 12.80 | 15.10 | 15.23 |
| Active optical fronthaul | | | |
| 0 | 12.80 | 15.10 | 15.23 |
| 9.91 | 12.80 | 15.10 | 15.23 |
| 18.46 | 12.80 | 15.10 | 15.23 |
| 21.76 | 12.80 | 15.10 | 15.23 |

in the downstream direction, with higher values shown by the wider BW.⁴⁶ Nonetheless, it is interesting to note that the percent deviation values between the theoretical and measured throughput are similar for different BWs (10 and 15 MHz). These percent deviations must be reduced in the future to improve the network performance of the SDR-based C-RAN architecture. In this sense, the origin of these differences between the theoretical and measured throughput must be also analyzed in detail considering other BW values and more UEs connected to the same USRP radio because these analyses can provide more information about the

Table 4 Throughput for **downstream** transmission using a radio as UE in the C-RAN architecture with an active and passive optical fronthaul with different fiber lengths. The UE consists of a radio (USRP B210) that transmits to the RRH 1 with a **BW = 15 MHz** channel. A comparison between theoretical and measured throughput is also shown.

| Optical fronthaul length (km) | Measured throughput in the cellular network (Mb/s) | Theoretical throughput based on the LTE standard (Mb/s) | Percent deviation between theoretical and measured throughput (%) |
|-------------------------------|--|---|---|
| Passive optical fronthaul | | | |
| 0 | 51.70 | 57.17 | 9.58 |
| 9.91 | 52.07 | 57.17 | 8.93 |
| 18.46 | 52.20 | 57.17 | 8.70 |
| 21.76 | 51.80 | 57.17 | 9.40 |
| Active optical fronthaul | | | |
| 0 | 51.70 | 57.17 | 9.58 |
| 9.91 | 51.27 | 57.17 | 8.93 |
| 18.46 | 51.47 | 57.17 | 8.70 |
| 21.76 | 52.27 | 57.17 | 9.40 |

Table 5 Throughput for **upstream** transmission using a radio as UE in the C-RAN architecture with an active and passive optical fronthaul with different fiber lengths. The UE consists of a radio (USRP B210) that transmits to the RRH 1 with a **BW = 15 MHz** channel. A comparison between theoretical and measured throughput is also shown.

| Optical fronthaul length (km) | Measured throughput in the cellular network (Mb/s) | Theoretical throughput based on the LTE standard (Mb/s) | Percent deviation between theoretical and measured throughput (%) |
|-------------------------------|--|---|---|
| Passive optical fronthaul | | | |
| 0 | 18.90 | 22.40 | 15.62 |
| 9.91 | 18.90 | 22.40 | 15.62 |
| 18.46 | 18.90 | 22.40 | 15.62 |
| 21.76 | 18.90 | 22.40 | 15.62 |
| Active optical fronthaul | | | |
| 0 | 18.90 | 22.40 | 15.62 |
| 9.91 | 18.83 | 22.40 | 15.92 |
| 18.46 | 18.90 | 22.40 | 15.62 |
| 21.76 | 18.90 | 22.40 | 15.62 |

capabilities and limitations of the SDR technology to manage a C-RAN architecture based on USRP X310 radios and employing the SRS open-source software. In any case, the deviations cannot be directly ascribed to the fronthaul configuration since these deviations are more likely to be attributed to the modulation and coding scheme (MCS) employed by the UE according to the RF received strength signal.

To extend our results, we consider the use of commercial cellphones (Xiaomi[®] Redmi 9A) as UEs in the cellular network. Table 6 presents the theoretical and measured throughput, which are

Table 6 Throughput for **downstream** and **upstream** transmissions using one cellphone as UE in the C-RAN architecture with an active optical fronthaul 21.76 km long. The UE consists of a cellphone (Redmi 9A, Xiaomi[®]) named UE 1 that transmits to the RRH 1 with a **BW = 10 MHz** channel. A comparison between theoretical and measured throughput is also shown.

| UE | Total throughput measured in the cellular network (Mb/s) | Theoretical throughput based on the LTE standard (Mb/s) | Percent deviation between theoretical and measured throughput (%) |
|------------|--|---|---|
| Downstream | | | |
| UE 1 | 35.00 | 38.01 | 7.99 |
| Upstream | | | |
| UE 1 | 12.80 | 15.10 | 15.23 |

obtained by considering one cellphone (named UE 1) connected to the RRH 1 with a BW = 10 MHz channel (Fig. 1). These measurements cannot be repeated for BW = 15 MHz because the commercial cellphones that we used do not support bandwidth values higher than 10 MHz. In addition, the results shown in Table 6 for downstream and upstream transmissions only correspond to the case of an active optical fronthaul of 21.76 km. Following the trend observed in Tables 2–5, very similar results are obtained for shorter fiber lengths. The throughput measurements carried out in the passive fronthaul for all fiber lengths led to practically the same results and hence they were omitted. In this sense, the results shown in Table 6 once again exhibit the important characteristic of independence of the fronthaul length or the type of fronthaul (active or passive) used in the C-RAN architecture.

If we compare the results shown in Table 6 with those shown in Tables 2 and 3 for 21.74 km of fronthaul length, we note that the throughput measurements have similar values when we use a cellphone instead of a USRP B210 as UE. In addition, the differences between the theoretical and measured throughput shown in Table 6 are 7.99% for downstream and 15.23% for upstream, which are very close to those reported in Tables 2 and 3. It is worth mentioning that the results shown in Tables 2, 3, and 6 are very similar to those shown in Ref. 51 between a USRP B210 acting as UE and two different commercial cellphones, where throughput values of 33 to 34 Mb/s and 13 to 14 Mb/s for downstream and upstream transmissions were reported using a BW = 10 MHz channel and the iPerf[®] tool respectively.

To obtain more insight into the throughput values in upstream and downstream transmissions, we increased the number of cellphones connected to the RRH 1. Table 7 shows the theoretical and measured throughput obtained when two identical commercial cellphones (named UE 1 and UE 2) are connected to the RRH 1 using a BW = 10 MHz channel. Again, in Table 7,

Table 7 Throughput for **downstream** and **upstream** transmissions using two cellphones as UEs in the C-RAN with an active fronthaul 21.76 km long. The UEs are two cellphones (Xiaomi[®] Redmi 9A) named UE1 and UE2, which transmit to the same RRH 1 with a **BW = 10 MHz** channel. A comparison between theoretical and measured throughput is shown.

| UE | Bitrate measured with iPerf (Mb/s) | Total throughput measured in the cellular network (Mb/s) | Theoretical throughput based on the LTE standard (Mb/s) | Percent deviation between theoretical and measured throughput (%) |
|------------|------------------------------------|--|---|---|
| Downstream | | | | |
| UE 1 | 10.33 | 30.66 | 33.67 | 8.92 |
| UE 2 | 20.33 | | | |
| Upstream | | | | |
| UE 1 | 3.63 | 11.94 | 12.00 | 0.54 |
| UE 2 | 8.31 | | | |

Table 8 Throughput for **downstream** and **upstream** transmissions using four cellphones as UEs in the C-RAN with an active optical fronthaul 21.76 km long. The UEs consist of four cellphones (Xiaomi[®] Redmi 9A), which transmit to the same RRH 1 with a **BW = 10 MHz** channel. A comparison between theoretical and measured throughput is also shown.

| UE | Bitrate measured with iPerf (Mb/s) | Total throughput measured in the cellular network (Mb/s) | Theoretical throughput based on the LTE standard (Mb/s) | Percent deviation between theoretical and measured throughput (%) |
|------------|------------------------------------|--|---|---|
| Downstream | | | | |
| UE 1 | 8.14 | 28.79 | 29.05 | 0.08 |
| UE 2 | 7.09 | | | |
| UE 3 | 6.91 | | | |
| UE 4 | 6.65 | | | |
| Upstream | | | | |
| UE 1 | 3.49 | 14.36 | 15.10 | 4.90 |
| UE 2 | 3.52 | | | |
| UE 3 | 3.27 | | | |
| UE 4 | 4.08 | | | |

only the results for downstream and upstream corresponding to the case of an active fronthaul of 21.76 km are displayed. This is because, in agreement with Tables 2 and 3, the results do not appreciably change when we employ shorter fronthaul lengths or a passive (instead of active) fronthaul. In Table 7, we note that both cellphones UE 1 and UE 2 do not present a balanced bit rate, but the sum of these bit rates, which correspond to the total throughput, present similar (downstream) and lower deviations (upstream) with respect to the theoretical throughput in comparison to the results shown in Table 6.

Now, we continue analyzing the throughput considering four and eight cellphones connected to the RRH 1. The corresponding results of these scenarios are shown in Tables 8 and 9, respectively. The aim of analyzing these scenarios is to evaluate the maximum quantity of UEs that can be connected using the USRP X310 radio (employed as RRH 1) in the C-RAN architecture.

According to Table 8, the four cellphones identified as UE 1, UE 2, UE 3, and UE 4 present a balanced bit rate distribution in comparison to the results shown in Table 7, where only two UEs are considered. In addition, the total throughput shown in Table 8, which corresponds to the sum of the bit rates obtained with all UEs, present lower percent deviations with respect to the theoretical throughput in comparison to those shown in Table 6. At this point, it seems that when the USRP X310 radios are connected to a higher number of UEs, a more stable and efficient operation in the C-RAN architecture is observed.

In contrast, with respect to the results shown in Table 9, we can observe that the eight UEs do not present a balanced bit rate, and the differences between the theoretical and the total measured throughput are not improved in comparison to the results shown in Table 8 for a lower number of UEs. In fact, we obtain a worse percent deviation in the upstream transmission. We attribute these worse results in throughput to the fact that we might be reaching the maximum capacity of the USRP X310 radio to support multiple UEs. Another reason is related to the position of the UEs with respect to the RRH. In this scenario, we intended placing all the eight cellphones together at 1 m distance from the RRH; however, as it is expected, some cellphones lie further away from the RRH than others. Another possible reason is related to the way the eNodeB performs the communication between the UEs with the RRH. In this sense, the eNodeB scheduler may not adequately realize the resource allocation among all UEs in both upstream and downstream transmissions. According to these observations, further throughput measurements must be performed in future works considering a higher number of UEs placed at different

Table 9 Throughput for **downstream** and **upstream** transmissions using eight cellphones as UEs in the C-RAN with an active optical fronthaul 21.76 km long. The UEs consist of eight cellphones (Xiaomi® Redmi 9A), which transmit to the same RRH 1 with a **BW = 10 MHz** channel. A comparison between theoretical and measured throughput is also shown.

| UE | Bitrate measured with iPerf (Mb/s) | Total throughput measured in the cellular network (Mb/s) | Theoretical throughput based on the LTE standard (Mb/s) | Percent deviation between theoretical and measured throughput (%) |
|------------|------------------------------------|--|---|---|
| Downstream | | | | |
| UE 1 | 5.87 | 33.49 | 33.67 | 0.53 |
| UE 2 | 4.20 | | | |
| UE 3 | 3.99 | | | |
| UE 4 | 3.37 | | | |
| UE 5 | 4.25 | | | |
| UE 6 | 3.45 | | | |
| UE 7 | 3.73 | | | |
| UE 8 | 4.64 | | | |
| Upstream | | | | |
| UE 1 | 3.49 | 6.41 | 12 | 46.6 |
| UE 2 | 3.52 | | | |
| UE 3 | 3.27 | | | |
| UE 4 | 4.08 | | | |
| UE 5 | 1.06 | | | |
| UE 6 | 0.82 | | | |
| UE 7 | 0.70 | | | |
| UE 8 | 0.68 | | | |

positions with respect to the same RRH to evaluate the scalability of the proposed C-RAN architecture based on these USRP X310 radios.

To follow with the assessment of the C-RAN architecture based on SDR using an active and passive optical fronthaul, we proceed to evaluate the following challenging transmission scenario, which consists of simultaneously operate four RRHs in the C-RAN architecture with two cellphones attached to each of them. To avoid overlapping connections of the cellphones to noncorresponding RRHs, every RRH is placed at least 5 m apart from each other and is operated with different radio frequencies. In addition, all frequency bands (in 2.5 and 2.6 GHz) used in the RRH (USRP) devices for the performance analysis were free bands that are still in the licensed process of the Mexican Federal Telecommunications Institute or unused by the cellular network operator. In particular, the RRH 1 operates at 2625 MHz for downstream and 2505 MHz for upstream, the RRH 2 operates at 2645 MHz for downstream and 2525 MHz for upstream, the RRH 3 operates at 2665 MHz for downstream and 2545 MHz for upstream, and finally, the RRH 4 operates at 2685 MHz for downstream and 2565 MHz for upstream. A frequency sweep was made with the use of a spectrum analyzer in all the LTE frequency division duplexing FDD band 7 (1620 to 1690 MHz for downlink) to guarantee the free-interference condition at the test ambient. The throughput measurements considering this scenario are shown in Tables 10 and 11 for downstream and upstream transmissions, respectively. In a similar way to Tables 6 and 7, the throughput results shown in Tables 10 and 11 were obtained considering an active optical fronthaul of 21.76 km. The throughput measurements carried out in the passive fronthaul and for

Table 10 Throughput for downstream transmission using two cellphones as UEs in each RRH installed in the C-RAN with an active optical fronthaul 21.76 km long and using a BW = 10 MHz channel. The UEs consist of commercial cellphones (Redmi 9A, Xiaomi®). A comparison between theoretical and measured throughput is also shown.

| RRH | UE | Bitrate measured with iPerf (Mb/s) | Total throughput measured in the cellular network (Mb/s) | Theoretical throughput based on the LTE standard (Mb/s) | Percent deviation between theoretical and measured throughput (%) |
|-------|------|------------------------------------|--|---|---|
| RRH 1 | UE 1 | 16.33 | 31.86 | 33.67 | 5.37 |
| | UE 2 | 15.53 | | | |
| RRH 2 | UE 1 | 13.93 | 31.23 | 33.67 | 7.24 |
| | UE 2 | 17.30 | | | |
| RRH 3 | UE 1 | 9.69 | 28.29 | 29.05 | 2.63 |
| | UE 2 | 18.60 | | | |
| RRH 4 | UE 1 | 27.03 | 39.20 | 41.34 | 5.16 |
| | UE 2 | 12.17 | | | |
| TOTAL | | 130.58 | | | |

Table 11 Throughput for upstream transmission using two cellphones as UEs in each RRH installed in the C-RAN with an active optical fronthaul 21.76 km long and using a BW = 10 MHz channel. The UEs consist of commercial cellphones (Redmi 9A, Xiaomi®). A comparison between theoretical and measured throughput is also shown.

| RRH | UE | Bitrate measured with iPerf (Mbits/s) | Total throughput measured in the cellular network (Mbits/s) | Theoretical throughput based on the LTE standard (Mbits/s) | Percent deviation between theoretical and measured throughput (%) |
|-------|------|---------------------------------------|---|--|---|
| RRH 1 | UE 1 | 6.67 | 13.44 | 15.01 | 10.46 |
| | UE 2 | 6.77 | | | |
| RRH 2 | UE 1 | 6.74 | 13.48 | 15.01 | 10.17 |
| | UE 2 | 6.74 | | | |
| RRH 3 | UE 1 | 6.84 | 13.61 | 15.01 | 9.30 |
| | UE 2 | 6.77 | | | |
| RRH 4 | UE 1 | 3.29 | 13.59 | 15.01 | 9.46 |
| | UE 2 | 10.3 | | | |
| TOTAL | | 54.13 | | | |

shorter fiber lengths led to practically the same results and again they were omitted. According to Fig. 1, we used the DWDM optical channels 28, 30, 32, and 34 to communicate the radios RRH 1, RRH 2, RRH 3, and RRH 4 with the eNodeB 1, eNodeB 2, eNodeB 3, and eNodeB 4, respectively. The throughput measurements shown in Tables 10 and 11 for each RRH are colored in red, green, blue, and purple in correspondence to the colored DWDM channels 28, 30, 32, and 34, as described in Fig. 1.

In general, we can observe from Tables 10 and 11 that for each RRH, their respective UEs present different measured bit rates, except for RRH 2 in upstream transmission. This unbalance in throughput for each UE again is attributed to the position of both UEs with respect to the RRH

and the way the eNodeB performs the link channel estimation between the UEs with the RRH. We also identify that for each RRH, the sum of the bit rates for UE 1 and UE 2 that correspond to the total throughput is maintained practically constant for all RRHs, and it occurs in both downstream and upstream transmissions. The only inconsequential exception might be RRH4 in downstream direction. Further, the total throughput per RRH obtained in Tables 10 and 11 does not exhibit large differences in comparison to their respective theoretical throughput values, especially in the downstream case. Moreover, these throughput differences given in percent deviations in Tables 10 and 11 are lower than those shown in Table 6, hence indicating a correct operation of the DWDM active and passive fronthaul to communicate the four USRP X310 radios with their respective four eNodeBs, at different DWDM wavelengths in the C-RAN architecture. In fact, for either upstream and downstream transmission, every RRH is connected, sharing the same optical fiber, to its corresponding eNodeB by setting up a different logical connection via different wavelengths. The optical channel independence is guaranteed by the extremely low linear and nonlinear cross-talk exhibited by the fronthaul as discussed in Sec. 2.

5 Discussion

It is interesting to remark that the throughput measurements and consequently the differences between theoretical and measured throughput observed in Tables 10 and 11 for both upstream and downstream transmissions, do not depend on the fronthaul length, the type of fronthaul employed (either active or passive), or the number of RRHs activated in the C-RAN architecture. Based on these observations, we can also state that the effect of using different DWDM channels in Tables 10 and 11 have no influence on the throughput measurements and that we could have even exchange the wavelength assigned to each RRH-eNodeB connection with no consequences to the network performance. With this analysis, we can confirm the suitability of the proposed C-RAN architectures described in Figs. 1 and 2 to scale the number of UEs and RRHs by correspondingly varying the number of DWDM lanes, setting up effectively independent logical connections between every RRH and eNodeB. This increment in transmission capacity can be observed in the total value obtained by the sum of the measured bit rates given in Tables 10 and 11 for downstream (130.50 Mbits/s) and upstream (50.13 Mbits/s), respectively. According to these results, it is expected that, by considering multiple DWDM channels transmitting at higher bit rates, the proposed active and passive fronthaul will present no problem to reach the high data transmission capacity required in 5G C-RAN systems.

Additionally, as a standard procedure to demonstrate the technical feasibility of an optical link, we analyze the power budget of the active and passive DWDM fronthaul architectures. To perform this analysis, we consider the error-free receiver sensitivity ($BER < 1 \times 10^{-12}$) specified in the datasheets of the colored DWDM transceivers employed in the active and passive C-RAN architecture for a maximum transmission rate of 10.3 Gb/s. According to Table 1, in the active scheme, we used DWDM transceivers for channels 28, 30, 32, and 34 provided by PacketLight® with sensitivity values of -16 dBm, whereas, in the passive fronthaul, we used DWDM transceivers for channels 29 and 33 provided by SolidOptics® with sensitivities of -24 dBm, and DWDM transceivers for channels 31 and 35 provided by SmartOptics® with sensitivities of -15 dBm, respectively. These values, together with the nominal and measured output optical power of each kind of transceiver, are displayed in Table 12. The available power budget (rightmost column) is then calculated as the difference between the minimum measured output power and the nominal sensitivity reported by each supplier. According to the loss analysis described in Sec. 2, for the complete active and passive fronthaul, including the optical fiber link of 21.76 km long and both MUX/DEMUX components, we obtain accumulative losses of 14.2 and 14.4 dB for upstream and downstream transmissions, respectively. By comparing these losses with the power budgets reported in Table 12, we observe that in the worst case, we still have a margin of $16.2 - 14.4$ dB = 1.8 dB to guarantee error-free operation in both configurations. Given the physical characteristics of the optical link, we are assuming null power penalties due to dispersion, nonlinearities, and available bandwidth. Still, >1 dB is available to allocate other penalties. Although our systems fulfill the power budget requirements, (if required) it is always possible to extend the system's reach by incorporating a semiconductor optical amplifier (SOA) prior to the DEMUX stage to extend the calculated margin or allocate further penalties.

Table 12 Available power budget for the different DWDM transceivers employed in this work. PacketLight transceivers are used for the active configuration, whereas SolidOptics® (channels 29 and 33) and SmartOptics® (channels 31 and 35) are used for the passive configuration.

| DWDM transceiver | Nominal sensitivity (dBm) | Nominal output power (dBm) | Minimum measured output power (dBm) | Available power budget (dB) |
|------------------|---------------------------|----------------------------|-------------------------------------|-----------------------------|
| PacketLight® | -16 | -1 to 3 | 1.0 | 17 |
| SolidOptics® | -24 | -1 to 5 | 0.4 | 24.4 |
| SmartOptics® | -15 | -1 to 4 | 1.2 | 16.2 |

According to our calculations, the impact on system performance of introducing the SOA would be negligible while boosting the power by at least 10 dB. This is possible due to the high operating OSNR of the analyzed systems, thus admitting the insertion of a large noise figure amplifier, and the low powers involved as compared to the input saturation power of current SOA devices, thus precluding its nonlinear behavior. In addition, by comparing Figs. 1 and 2, we note that the DWDM channels in the passive scheme are transmitted along two additional patch cords (10 m long) with their respective connectors in comparison to the active fronthaul scheme. These additional components produce an increment of the losses in the passive optical fronthaul of maximum 0.3 dB, posing no problem for the passive C-RAN architecture despite the sub-optimum conditions of the optical fiber link. These findings also put forward the proposed DWDM passive fronthaul, in comparison with the active scheme, as a viable, less complex, and cost-sensitive solution for C-RAN with fronthaul lengths up to, practically, 22 km. At this point, it is important to comment on the importance to maintain the optical fiber connectors clean in all the mechanical splices found in the optical link, because a dirty or contaminated connector can increase the losses and exceed the power budget limit in both active and passive optical fronthaul configurations.

With respect to the latency characteristics of the optical active and passive fronthaul, we have to take into account the delay budget established for 5G systems, which must comply a maximum round-trip delay of $\sim 250 \mu\text{s}$ between the RRH and BBU, including the optical fiber propagation delay and additional processing delays caused by other fronthaul's components.²⁵⁻³⁰ This in turn sets a constraint on the maximum optical fiber length employed in the fronthaul architecture. If we assume a $5 \mu\text{s}/\text{km}$ light propagation delay in the optical fiber link, then, for 21.76 km we have a round trip delay of $217.6 \mu\text{s}$. The MUX/DEMUX components employed in the active and passive fronthaul do not appreciably increase this round-trip delay, but the transponder equipment employed in the active optical fronthaul can increase this value. According to Refs. 54 and 55, the transponders PL1000TE employed in the active fronthaul show low latency operation with maximum processing delays of $10 \mu\text{s}$. Therefore, the active optical fronthaul configuration, which employs two of these transponders and uses 21.76 km of fiber length, can reach a maximum round-trip delay of $237.6 \mu\text{s}$. For the passive optical fronthaul, which only employs 21.76 km of fiber length, the maximum round-trip delay is kept at $217.6 \mu\text{s}$. According to these latency estimations, it is expected that both active and passive fronthaul configurations can satisfy the latency conditions required for 5G C-RAN architectures.

Finally, it is important to analyze the viability to integrate these fronthaul configurations in coexisting 4G/5G systems based on SDR. At this point, the active and passive DWDM fronthaul configurations analyzed in this work allow this coexistence since both fronthaul configurations can support the capacity and latency conditions required to operate both 4G and 5G C-RAN architectures. In this context, the SDR technology employed in this work has the potential to offer reconfigurable low-cost operation of coexisting 4G and 5G C-RAN architectures because it can modify the programmed functions of the multiple USRP radios and eNodeBs used in the C-RAN architecture to simultaneously operate in 4G and 5G, according to the mobile traffic demand present in the coverage area. Nevertheless, the SDR technology that employs the SRS open-source software still needs to be evaluated in detail for 5G standalone and nonstandalone operations. The analysis of this open issue in combination with hybrid active and passive optical fronthaul configurations of different fiber lengths still represents work in progress.


6 Conclusions

We perform a comparative analysis of an active and passive optical fronthaul with DWDM technology, and we discuss the viability of these fronthaul configurations to be employed in a 4G/5G C-RAN architecture based on the use of software-defined radios. We experimentally demonstrate the feasibility of the active and passive optical fronthaul to communicate the srs-RRHs with their respective srs-eNodeBs through a DWDM optical link with lengths slightly longer than 20 km in a 4G C-RAN architecture. In addition, we verify that both active and passive DWDM fronthaul schemes are adequate to scale up the number of UEs and RRH's in the C-RAN architecture by using different DWDM channels, thus increasing the transmission capacity of the cellular network. We also report the throughput measurements generated in the C-RAN architecture using the active and passive DWDM optical fronthaul, and we show that the DWDM channels used in both optical fronthaul schemes have no influence in these throughput measurements despite the high optical losses present in the employed optical link, which are around 14.2 and 14.4 dB for the downstream and upstream directions, respectively. In addition, our findings put forward the proposed DWDM passive fronthaul, in comparison with the active scheme, as a viable, less complex, and cost-sensitive solution for CRAN systems with fronthaul lengths up to 21.76 km. All these results and the experiences reported on the C-RAN implementation provide valuable information to design and develop future 4G and 5G C-RAN architectures based on software-defined radios operating simultaneously in a shared DWDM optical fronthaul infrastructure with the capability to manage a variety of user traffic demands.

Acknowledgments

This work has been supported by the Government of Mexico City through project SECTEI/200/2019, and by the Dir. Gral. Asuntos Personal Académico - UNAM, through PAPIIT project IN104720. Also, the authors are grateful to the Institute of Engineering and the School of Engineering at UNAM-Mexico for their assistance in the development of this research work.

References

1. Ericsson, "Ericsson mobility report June 2020," 2020, <https://www.ericsson.com/49da93/assets/local/mobility-report/documents/2020/june2020-ericsson-mobility-report.pdf>.
2. L. Wan, Z. Guo, and X. Chen, "Enabling efficient 5G NR and 4G LTE coexistence," *IEEE Wireless Commun.* **26**(1), 6–8 (2019).
3. A. O. Mufutau et al., "Demonstration of a hybrid optical fiber–wireless 5G fronthaul coexisting with end-to-end 4G networks," *J. Opt. Commun. Netw.* **12**(3), 72–78 (2020).
4. Cisco, "Cisco annual internet report (2018–2023)," 2020, http://grs.cisco.com/grsx/cust/grsCustomerSurvey.html?SurveyCode=4153&ad_id=US-BN-SEC-M-CISCOSECURITYRPT-ENT&KeyCode=000112137. 
5. M. A. Habibi et al., "A comprehensive survey of RAN architectures toward 5G mobile communication system," *IEEE Access* **7**, 70371–70421 (2019).
6. M. Agiwal, A. Roy, and N. Saxena, "Next generation 5G wireless networks: a comprehensive survey," *IEEE Commun. Surv. Tutorials* **18**(3), 1617–1655 (2016).
7. I. A. Alimi, A. L. Teixeira, and P. P. Monteiro, "Toward an efficient C-RAN optical fronthaul for the future networks: a tutorial on technologies, requirements, challenges, and solutions," *IEEE Commun. Surv. Tutorials* **20**(1), 708–769 (2018).
8. D. H. Hailu et al., "Mobile fronthaul transport options in C-RAN and emerging research directions: a comprehensive study," *Opt. Switch. Networking* **30**, 40–52 (2018).
9. X. Liu and F. Effenberger, "Emerging optical access network technologies for 5G wireless [invited]," *J. Opt. Commun. Networking* **8**, (12), B70–B79 (2016).
10. G. Kalfas et al., "Next generation fiber-wireless fronthaul for 5G mmWave networks," *IEEE Commun. Mag.* **57**(3), 138–144 (2019).
11. C. Ranaweera et al., "5G C-RAN with optical fronthaul: an analysis from a deployment perspective," *J. Lightwave Technol.* **36**(11), 2059–2068 (2018).

12. B. Skubic et al., "Optical transport solutions for 5G fixed wireless access [Invited]," *J. Opt. Commun. Networking* **9**(9), D10–D18 (2017).
13. J. (Shihuan) Zou et al., "Advanced optical access technologies for next-generation (5G) mobile networks [Invited]," *J. Opt. Commun. Networking* **12**(10), D86–D98 (2020).
14. J. Zou et al., "Recent trials of G.metro-based passive WDM fronthaul in 5G testbeds," in *IEEE Int. Conf. Commun. Work. ICC Workshops 2019 - Proc.*, pp. 1–6 (2019).
15. ITU-T, "Recommendation ITU-T G.698.4: multichannel bi-directional DWDM applications with port agnostic single-channel optical interfaces," 2018, <https://www.itu.int/rec/T-REC-G.698.4/en>.
16. F. Musumeci et al., "Optimal BBU placement for 5G C-RAN deployment over WDM aggregation networks," *J. Lightwave Technol.* **34**(8), 1963–1970 (2016).
17. N. Suzuki et al., "100 Gb/s to 1 Tb/s based coherent passive optical network technology," *J. Lightwave Technol.* **36**(8), 1485–1491 (2018).
18. A. D. Hossain and A. R. Hossain, "A distributed control framework for TDM-PON based 5G mobile fronthaul," *IEEE Access*, **7**, 162102–162114 (2019).
19. A. F. Y. Mohammed et al., "A green converged TWDM-PON and 5G HetNet catering applications demanding low latency," *Opt. Fiber Technol.* **58**, 102261 (2020).
20. J. Zhang et al., "Low latency DWBA scheme for mini-slot based 5G new radio in a fixed and mobile converged TWDM-PON," *J. Lightwave Technol.* **40**(1), 3–13 (2022).
21. J. M. Galve et al., "Reconfigurable radio access networks using multicore fibers," *IEEE J. Quantum Electron.* **52**(1), (2016).
22. S. Rommel et al., "High-capacity 5G fronthaul networks based on optical space division multiplexing," *IEEE Trans. Broadcast.* **65**(2), 434–443 (2019).
23. N. Amaya et al., "Software defined networking (SDN) over space division multiplexing (SDM) optical networks: features, benefits and experimental demonstration," *Opt. Express*, **22**(3), 3638–3647 (2014).
24. M. Morant and R. Llorente, "Performance analysis of multiple radio-access provision in a multicore-fibre optical fronthaul," *Opt. Commun.* **436**, 161–167 (2019).
25. S. S. Jaffera et al., "A low cost PON-FSO based fronthaul solution for 5G CRAN architecture," *Opt. Fiber Technol.* **63**(2), 102500 (2021).
26. S. Matoussi, I. Fajjari, and S. Costanzo, "5G RAN: functional split orchestration optimization," *IEEE J. Sel. Areas Commun.* **38**(7), 1448–1463 (2020).
27. C. Ranaweera et al., "5G C-RAN architecture: a comparison of multiple optical fronthaul networks," in *Int. Conf. Opt. Network Design and Model. (ONDM)*, p. 1698131.
28. P. Iovana et al., "Future proof optical network infrastructure for 5G transport," *J. Opt. Commun. Networking* **8**(12), B80–B92 (2016).
29. J. Zhang et al., "Experimental demonstration of fronthaul flexibility for enhanced CoMP service in 5G radio and optical access networks," *Opt. Express* **25**(18), 21247–21258 (2017).
30. J. Zou et al., "Demonstration of X-haul architecture for 5G over converged SDN fiber network," in *Opt. Fiber Commun. Conf. and Expos. (OFC), INSPEC Accession Number: 17856300* (2018).
31. 3rd Generation Partnership Project, "Technical Specification Group Radio Access Network - Physical channels and modulation - Release 15," Technical Report 38.211 V15.8.0, 3GPP (2020).
32. L. Bonati et al., "Open, programmable, and virtualized 5g networks: state-of-the-art and the road ahead," *Comput. Networks* **182**, 107516 (2020).
33. W. Ejaz et al., "A comprehensive survey on resource allocation for CRAN in 5G and beyond networks," *J. Network Comput. Appl.* **160**, 102638 (2020).
34. M. Fiorani et al., "Transport abstraction models for an SDN-controlled centralized RAN," *IEEE Commun. Lett.* **19**(8), 1406–1409 (2015).
35. K. Ramantas et al., "A C-RAN based 5G platform with a fully virtualized, SDN controlled optical/wireless fronthaul," in *Int. Conf. Transparent Opt. Networks*, pp. 2018–2021 (2018).
36. The openairinterface initiative, "Openairinterface: The fastest growing community and software assets in 5G wireless," <http://www.openairinterface.org/> (2022).
37. Software Radio Systems SRS, "srsRAN: Your own mobile network," <http://www.srslte.com/> (2022).

38. F. Kaltenberger et al., “OpenAirInterface: democratizing innovation in the 5G Era,” *Comput. Networks* **176**, 107284 (2020).
39. Z. Geng et al., “Performance analysis and comparison of GPP-based SDR systems,” in *7th IEEE Int. Symp. Microwave, Antenna, Propag., and EMC Technol. (MAPE)*, Xi’an (2017).
40. D. M. Molla et al., “Software defined radio platforms for wireless technologies,” *IEEE Access* **10**, 26203–26229 (2022).
41. Ettus Research, “USRP hardware driver and USRP manual: USRP X3x0 series,” https://files.ettus.com/manual/page_usrp_x3x0.html (accessed 21 January 2021).
42. Ettus Research, “USRP hardware driver and USRP manual: USRP B2x0 series,” https://files.ettus.com/manual/page_usrp_b200.html (accessed 21 January 2021).
43. I. Gomez-Miguel et al., “srsLTE: an open-source platform for LTE evolution and experimentation,” in *Proc. ACM Intl. Workshop Wireless Network Testbeds, Exp. Eval. & Characterization (WiNTECH)*, New York (2016).
44. Software Radio Systems, “srsLTE documentation release 20.04.0,” https://docs.srsran.com/_downloads/en/rfsoc/pdf/ (2022).
45. ITU-T, “Recommendation ITU-T G.694.1: spectral grids for WDM applications: DWDM frequency grid,” 2012, <https://www.itu.int/rec/T-REC-G.694.1-201202-I/es>
46. ITU-T, “Recommendation ITU-T G.652: characteristics of a single-mode optical fibre and cable,” 2016, <https://www.itu.int/rec/T-REC-G.652-201611-I/en>.
47. Y. Song et al., “Simulation and experimental investigation of nonlinear effects in 5G fronthaul transmission system based on WDM-PON architecture,” *Opt. Fiber Technol.* **65**, 102628 (2021).
48. C. Matrakidis et al., “Analytical modeling of dispersion penalty for NRZ transmission,” in *Proc. 1st Int. Congr. Eng. Technol.*, 1st ed., pp. 1–6, CRC Press (2021).
49. J. Dugan et al., “iPerf - The TCP, UDP and SCTP network bandwidth measurement tool,” <https://iperf.fr/> (accessed 21 January 2021).
50. S. Iqbal and J. M. Hamamreh, “A comprehensive tutorial on how to practically build and deploy 5G networks using open-source software and general-purpose, off-the-shelf hardware,” *RS Open J. Innov. Commun. Tech.* **2**(6), 1–28 (2021).
51. F. Gringoli et al., “Performance assessment of open software platforms for 5G prototyping,” *IEEE Wireless Comm.* **25**(5), 10–15 (2018).
52. S. Pramanik, A. Ksentini, and C. F. Chiasserini, “Characterizing the computational and memory requirements of virtual RANs,” in *17th Wireless On-Demand Network Syst. and Serv. Conf. (WONS)*, Oppdal (2022).
53. S. Rathi et al., “Throughput for TDD and FDD 4G LTE systems,” *Int. J. Innov. Explor. Eng.* **3**, 2278–3075 (2014).
54. Packetlight Networks, “PL1000TE datasheet,” <https://www.packetlight.com//images/Data-Sheets/PL-1000TE.pdf> (2022).
55. V. Bobrovs, S. Spolitis, and G. Ivanovs, “Latency causes and reduction in optical metro networks,” *Proc. SPIE* **9008**, 90080C (2014).

Biographies of the authors are not available.

Queries

1. Please review the revised proof carefully to ensure your corrections have been inserted properly and to your satisfaction.
2. If any of your requested changes were not made on this revised proof, it's possible that they were in conflict with the journal's style. For example, author corrections to hyphenation, italics, and capitalization occasionally conflict with journal style. However, if you find that any corrections have been omitted that affect the technical content of your paper, please contact journals@spie.org and also include those corrections in your author response to the proofs.

Funding Information

The authors have identified the following funders and award numbers, either on the submission form at the time of submission or in the Acknowledgments of the manuscript. Please check this list of funding agencies and make any necessary corrections using the full and official name of the funding organization. You may also wish to edit the Acknowledgments, if needed. This information may be used to help SPIE comply with funding reporting mandates.

- Government of Mexico City Through Project; Award no. SECTEI/200/2019
- Dir. Gral. Asuntos Personal Académico - UNAM, Through PAPIIT Project; Award no. IN104720